JACS
JOURNAL OF THE AMERICAN CHEMICAL SOCIETY

Communication

pubs.acs.org/JACS

Nanoscale Electrochemical Patterning Reveals the Active Sites for Catechol Oxidation at Graphite Surfaces

Anisha N. Patel,[†] Kim McKelvey,[†,‡] and Patrick R. Unwin*[,†]

[†]Department of Chemistry and [‡]MOAC Doctoral Training Centre, University of Warwick, Coventry CV4 7AL, United Kingdom

Supporting Information

ABSTRACT: Graphite-based electrodes (graphite, graphene, and nanotubes) are used widely in electrochemistry, and there is a long-standing view that graphite step edges are needed to catalyze many reactions, with the basal surface considered to be inert. In the present work, this model was tested directly for the first time using scanning electrochemical cell microscopy reactive patterning and shown to be incorrect. For the electro-oxidation of dopamine as a model process, the reaction rate was measured at high spatial resolution across a surface of highly oriented pyrolytic graphite. Oxidation products left behind in a pattern defined by the scanned electrochemical cell served as surface-site markers, allowing the electrochemical activity to be correlated directly with the graphite structure on the nanoscale. This process produced tens of thousands of electrochemical measurements at different locations across the basal surface, unambiguously revealing it to be highly electrochemically active, with step edges providing no enhanced activity. This new model of graphite electrodes has significant implications for the design of carbon-based biosensors, and the results are additionally important for understanding electrochemical processes on related sp^2-hybridized materials such as pristine graphene and nanotubes.

Carbon electrodes, from graphite to conducting diamond, constitute interesting platforms for electroanalysis and electrocatalysis because of their low background currents, wide potential windows, chemical inertness, sensitivity, biocompatibility, low cost, and ready availability.[1] They have found particularly wide application in bioelectrochemical analysis, either directly or as supports for electrocatalysts.[2] The introduction of graphene and carbon nanotubes (CNTs) has expanded the range of carbon-based electrodes materials and enhanced the need for a greatly improved understanding of the electrochemical properties of graphitic materials.

Carbon electrodes are used extensively for the electrochemical detection and analysis of catechols[1,3] and related molecules, with apparently slow kinetics being found for dopamine (DA) electro-oxidation on basal-plane graphite, with peak-to-peak separations as large as 1.2 V (at 0.2 V s^{-1}) in cyclic voltammetry.[4] On this basis, such processes have been considered to be catalyzed solely by step edges, with the basal surface regarded as inert.[4,5] Consequently, carbon electrodes used in neuroscience and on biosensing platforms are often designed to maximize step edges.[1c,6] The studies reported herein show that this model is incorrect for the most studied neurotransmitter, DA. Rather, electrochemical oxidation is rapid on the basal surface of highly orientated pyrolytic graphite (HOPG), but the surface is rapidly poisoned by the electro-oxidation process, which causes the adsorption of polymeric material on the electrode. We were able to take advantage of this in scanning electrochemical cell microscopy (SECCM)[7] by designing patterning experiments in which the reaction is measured on an essentially pristine surface at high resolution but the SECCM probe leaves the blocking products behind as place markers when it moves on to a new location; these markers can then be found and analyzed by complementary microscopy.[8] This enables the electrochemical response to be correlated unambiguously to the location on the carbon electrode surface, revealing structure−activity correlations with unprecedented (nanoscale) resolution.

We first investigated the electro-oxidation of DA on the macroscale. With a Teflon cylinder that was gently placed on the HOPG surface to define a 3 mm diameter working electrode (WE), 10 consecutive cyclic voltammograms (CVs) were recorded at 5 s intervals for DA oxidation in 0.15 M phosphate buffered saline (PBS) containing 150 mM NaCl (pH 7.2) at 0.1 V s^{-1} with a Ag/AgCl (150 mM NaCl) reference electrode and Pt counter electrode. The highest-quality HOPG was used, originating from Dr. A. Moore of Union Carbide (now GE Advanced Ceramics), which was kindly provided by Prof. R. L. McCreery (University of Alberta, Canada). The HOPG was carefully cleaved immediately before use with a razor blade, as described previously.[4] As shown herein and outlined in past work,[4,9] this procedure and material provides very high quality surfaces with very low step densities and extensive basal terraces. Figure 1 shows typical CVs of (a) 1 mM and (b) 50 μM DA, with the first CV in each case recorded within 1 min after the HOPG was freshly cleaved. For 1 mM DA, the initial CV showed an apparent quasi-reversible electrochemical response with a peak-to-peak separation of 68 mV, that rapidly deteriorated over the course of subsequent measurements. The basal surface was rapidly contaminated, as evident from the decrease in peak current by 80% and the dramatic increase in the peak-to-peak separation to >280 mV after 10 cycles. In contrast, when the concentration was decreased to 50 μM, the initial peak-to-peak separation was 30 mV, and the extent to which the signal decayed over the following 10 cycles was diminished, although there was still some surface blocking, as detected by in situ AFM carried out concurrently with the voltammetry measurements. Figure 1c shows a typical image of the pristine surface of HOPG, and in 100

Received: September 27, 2012
Published: December 4, 2012

   dx.doi.org/10.1021/ja3095894 | J. Am. Chem. Soc. 2012, 134, 20246−20249

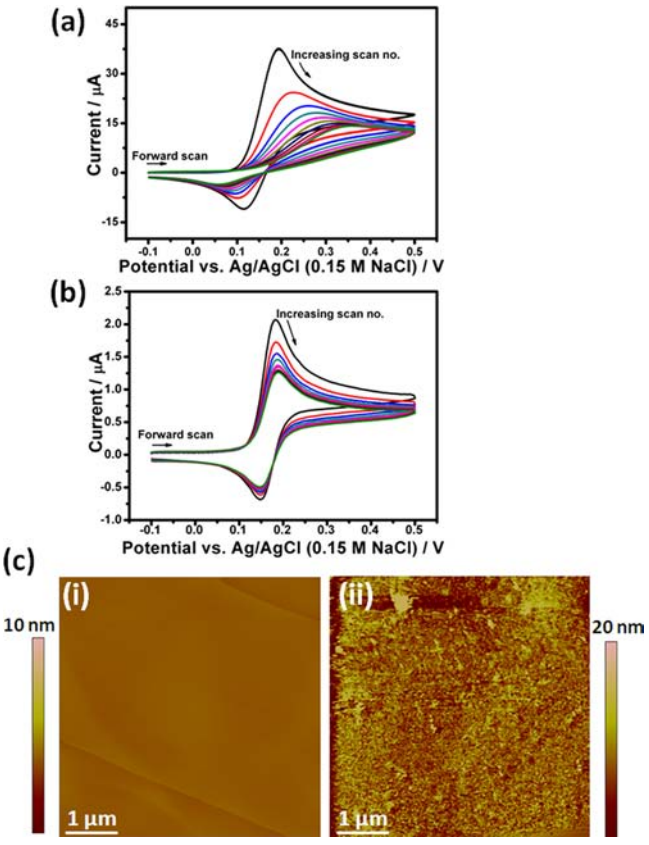

Figure 1. (a, b) CVs for the oxidation of (a) 1 mM and (b) 50 μM DA at 0.1 V s^{-1} on pristine basal-plane HOPG. (c) AFM images of HOPG: (i) pristine surface; (ii) in situ after one CV scan for 100 μM DA electro-oxidation between 0 and 0.45 V at 0.1 V s^{-1}.

μM DA (0.15 PBS, pH 7.2) after just one CV scan between the potential limits of 0 V (start and end potentials) and 0.45 V (reverse potential) at 0.1 V s^{-1}. The image shows coverage of the electrode surface by DA oxidation products formed via polymerization.[1c]

Although these macroscopic data could suggest that the basal surface of HOPG is actually highly electrochemically active, in contrast to previous work,[4,5] the evidence is not definitive because the electrode consisted of a basal surface intersected by step edges. Thus, to determine definitively the surface sites for DA electro-oxidation, we used SECCM[7a,b,10] to image an area of the HOPG with a distinctive line pattern so that the SECCM activity data could be compared with AFM and SEM measurements of the same area, allowing a direct correlation of the HOPG structure with the activity for DA electro-oxidation. For the studies reported first, a dual-channel borosilicate pipet pulled to a ~1 μm tapered end was filled with 100 μM DA in 0.15 M PBS containing 150 mM NaCl (pH 7.2), with a liquid meniscus formed at the end of the tip,[7b] and a Ag/AgCl quasi-reference counter electrode (QRCE) was inserted into each channel. The HOPG sample was mounted on a high-precision piezoelectric *xy* stage and connected as the WE. When the tip was lowered using a piezoelectric *z* positioner until the meniscus made contact with the WE, an electrochemical cell was formed[7a,b,8,10,11] (Figure S1 in the Supporting Information). A linear sweep voltammogram (LSV) was run using the SECCM setup before the patterning experiments; a typical example is shown in Figure 2a. The wave was sigmoidal, as expected for the SECCM format with a tapered pipet,[7b] and reached a limiting current of ca. 8 pA at ca. 0.3 V, a reasonable value on the basis of the pipet dimensions, diffusion coefficient, and DA concentration.[7b]

SECCM line patterning was first carried out at a substrate potential of 0.25 V vs Ag/AgCl (0.15 M NaCl), resulting in a current just below the maximum diffusion-limited value. A small oscillation of the tip position normal to the surface (20 nm peak amplitude, 233.6 Hz) was applied, giving rise to an alternating-conductance current (AC) across the meniscus due to periodic changes in the meniscus height. This AC (~65 pA) was used as a set point for feedback, enabling a constant tip-to-substrate separation during imaging. The direct ion conductance current (DC) between the two QRCEs (Figure S1) was ~3.2 nA. The resulting surface pattern is evident in Figure 2b–e: it covers 560 μm in length. The tip was scanned at a speed of 1 μm s^{-1} and 78 data points were recorded every second (each averaged over 512

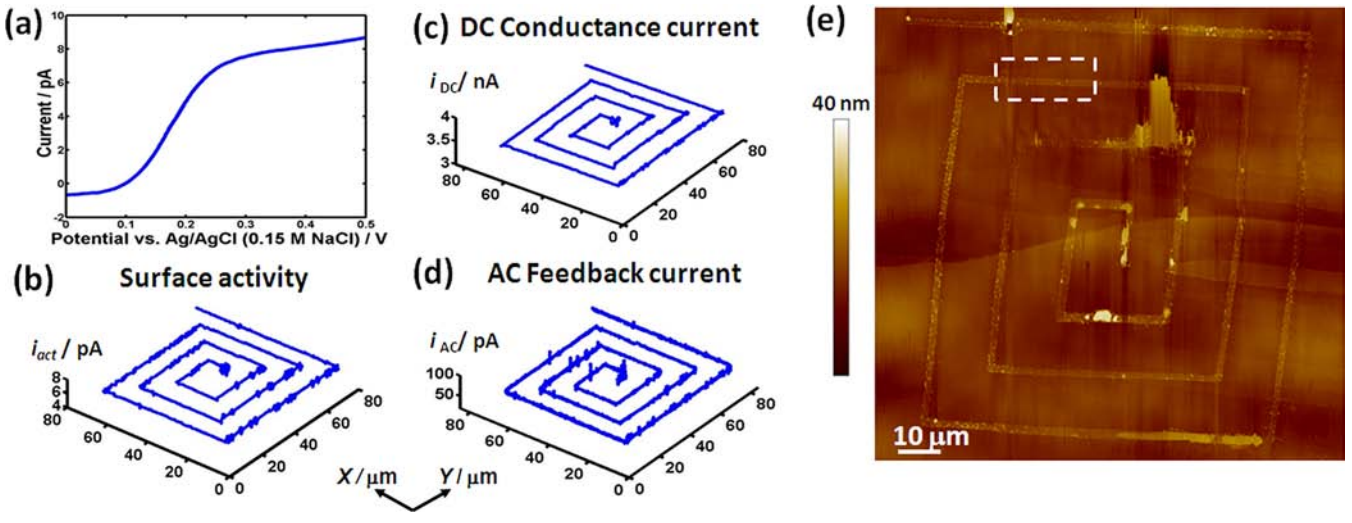

Figure 2. (a) SECCM LSV for the oxidation of 100 μM DA (0.15 M PBS) at 0.1 V s^{-1}. (b–d) SECCM reactive patterning maps for DA electro-oxidation: (b) surface activity; (c) DC component of the conductance current; (d) AC component of the conductance current used for feedback (see the text for details). (e) AFM image of the HOPG surface showing the SECCM deposited pattern.

dx.doi.org/10.1021/ja3095894 | *J. Am. Chem. Soc.* 2012, 134, 20246–20249

samples), resulting in a total of >40 000 individual measurements across the surface.

The SECCM surface activity map (Figure 2b) clearly shows that the HOPG surface currents were essentially constant at 6.4 ± 1.0 pA over the probed area (also see Figure S2 for a histogram of the activity data). The SECCM conductance currents (AC and DC; Figure 2c,d) were fairly constant, highlighting the fact that the probe was maintained at a fixed distance from the surface and that the mass transport was constant (also see Figure S2 for data histograms). There were some small features that coincided in the three current maps (Figure 2b–d) along the *y*-axis scan, corresponding to positions where the droplet encountered multilayer or monolayer steps, which caused small disruptions in the droplet size and surface interactions. However, these features are not significant. The simultaneously obtained topography map (tip position in *x*, *y*, and *z*; Figure S3) confirmed the imaging of the surface.

As highlighted earlier, a key feature of the approach described here is that the electro-oxidation of DA leads to the deposition of material, enabling the SECCM current activity to be linked unambiguously to the site on the WE. The AFM image in Figure 2e confirms that continuous deposition of the DA oxidative products occurred throughout the SECCM measurements. The occasional streaking in the region of the deposited film (where the topography appears higher) is due to sticking of the AFM tip, which dragged the film. This is not true topography and was not seen in the scanning electron microscopy image of the same area (Figure S4). Significantly, the AFM data showed that the deposition patterning (see Figure S5 for a magnified view of this region) was initiated on a basal-plane region that was at least 2 μm away from the nearest step edge. This region, in the center of the spiral, evidently had associated high electrochemical activity, indicating that the reactive patterning and corresponding HOPG electroactivity did not require a step defect but was solely due the electro-oxidation of DA on the basal plane.

More detailed AFM analysis on a section of the pattern (marked in white in Figure 2e) was carried out to allow the activity to be correlated with the HOPG surface structure. Figure 3a shows an AFM image of this region, and Figure 3b displays the corresponding surface activity (green) and DC component of the conductance current (blue). The AFM image shows that the deposited line traveled essentially exclusively on a basal terrace with no obvious step defects. The corresponding SECCM data show uniform surface activity that remained fairly constant at 6.5 ± 0.1 pA, as expected for a very active electrode surface.

Taken together, the data in Figure 3 show unequivocally that DA electro-oxidation occurs readily on the basal surface of HOPG, in complete contrast to the present model, which considers the basal surface to be inert, with step edges required to catalyze the reaction. For some other electrode materials, catechol adsorption has been shown to promote fast electron transfer;[12] to elucidate whether this was important for the basal surface of HOPG, we carried out SECCM "landing" transient chronoamperometric measurements in which the QRCEs in the pipet cell were biased at a value to promote DA oxidation when the meniscus came into contact with the pristine HOPG surface. Experiments were carried out with 10 μM DA to minimize any accumulation of DA on the surface. A typical transient, characteristic of 20 runs on fresh spots on a pristine HOPG (AM) surface, is shown in Figure S6. The redox current decayed to a steady value in a few hundred milliseconds, a time scale characteristic of diffusion in SECCM.[13] While this indicates facile electron transfer, we cannot rule out the involvement of DA

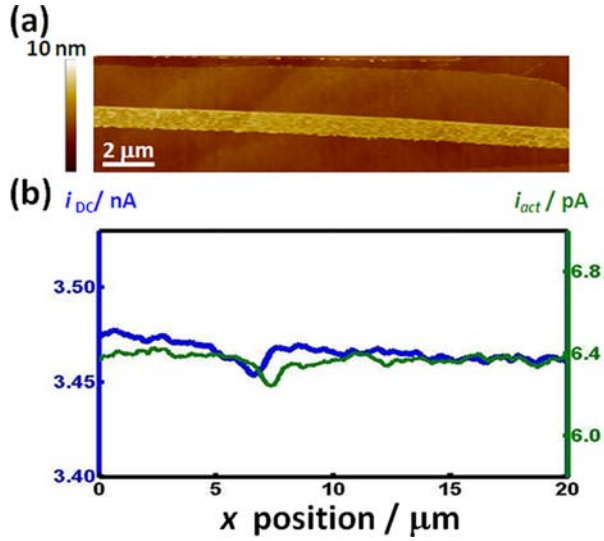

Figure 3. (a) AFM image (20 μm × 5 μm) of the section of the line patterning marked in white in Figure 2e. (b) Overlay of the corresponding surface activity (green) and DC component of the conductance current (blue).

adsorption, although the adsorption rate constant would need to be similar to or higher than that measured on other carbon electrodes.[12b]

We were next interested in elucidating whether there was any variation in activity between the basal surface and step edges, so SECCM reactive patterning was also carried out at a potential close to the half-wave potential, where any such variation would have been more readily evident. SECCM imaging was successful with 100 μM DA, but the diminished reaction flux meant that the electrodeposition was not sufficiently extensive for analysis by AFM. It should be noted that the result of this experiment also confirmed that the patterning was due to product adsorption and not the reactant. The concentration was thus increased to 300 μM. Figure 4a shows a typical line from DA electro-oxidation that traveled along a large basal terrace but also intersected several steps, ranging between 0.3 (monolayer) and 1.5 nm in height (see the AFM cross-section overlaid in red in Figure 4a). From the correlation of the AFM image with the DC component of the conductance current (blue) and the surface activity (green), as shown in Figure 4b, the following important points can be made. First, it can be seen that as the meniscus traveled along the basal terrace (ca. 9 μm long), the surface activity remained constant at ca. 11 pA, a value consistent with a highly active surface. Second, in the region of step edges, the surface current dropped slightly. Since the meniscus still mostly covered the basal surface in these regions, we attribute this to enhanced blocking of the surface in stepped regions on the SECCM time scale. It can be seen that the corresponding DC current (Figure 4b) was fairly uniform in this region, indicating that the mass transport rate was constant.

The major outcome of this study has been to show that electro-oxidation of the model catechol, DA, occurs readily on basal-plane HOPG, in contrast to the longstanding model picturing the basal plane as inert. However, the surface is easily contaminated by reaction products, which leads to rapid deactivation of the surface. SECCM reactive patterning is a new approach that provides an unequivocal and unambiguous correlation of surface structure and electrochemical activity. Of course, the basal surface itself contains point defects that may have different local ET activities. However, as we have pointed out elsewhere,[14] such

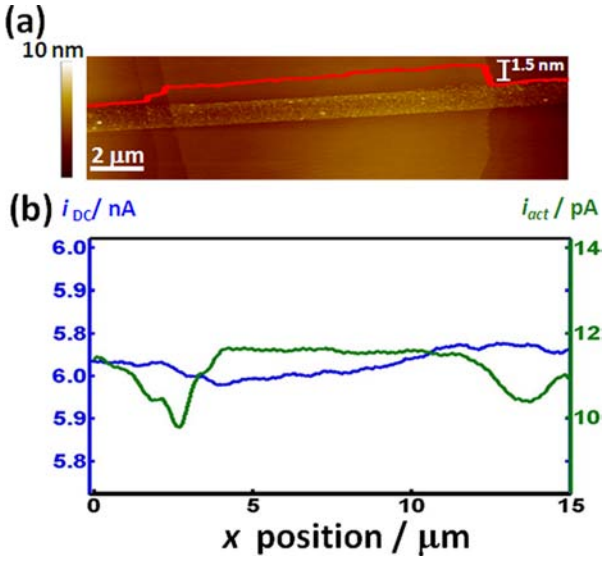

Figure 4. (a) AFM image (15 μm × 5 μm) of a section of line patterning carried out at the half-wave potential with 300 μM DA (0.15 M PBS). The AFM cross section is overlaid in red. (b) Overlay of the corresponding surface activity (green) and DC component of the conductance current (blue).

defects have never been considered necessary to explain the reactivity of HOPG. As the samples used for the studies herein were of the very highest quality in terms of low defect density,[14] our measurements represent the behavior of the best available pristine surface, which is essentially uniformly active on the SECCM scale. The approach provides a significant weight of evidence in the form of thousands of individual current measurements that can be attributed unequivocally to the basal surface.

This new view of complex electrochemical processes at graphite, together with other recent studies on simpler redox systems,[10,13,14] suggests that a significant reappraisal of graphite as an electrode material is needed. This has major implications for related sp^2-hybridized carbons, such as graphene and CNTs. More generally, this study adds to a growing body of work highlighting the considerable value of electrochemical patterning and imaging[15] as a means of understanding local surface activity.

■ ASSOCIATED CONTENT

Supporting Information

Additional SECCM, AFM, and SEM data. This material is available free of charge via the Internet at http://pubs.acs.org.

■ AUTHOR INFORMATION

Corresponding Author

p.r.unwin@warwick.ac.uk

Notes

The authors declare no competing financial interest.

■ ACKNOWLEDGMENTS

We are grateful to the European Research Council (ERC-2009-AdG 247143-QUANTIF) and thank the EPSRC for a studentship to A.N.P. (Analytical Fund EP/F064861/1e) and support for K.M. through funding of the MOAC Doctoral Training Centre. Some equipment used in this research was obtained through Birmingham Science City with support from Advantage West Midlands and the European Regional Development Fund. We thank Prof. R. L. McCreery for kindly providing the high-quality HOPG sample used herein and Dr. A. W. Colburn for designing and building electronic instrumentation.

■ REFERENCES

(1) (a) McCreery, R. L. *Chem. Rev.* **2008**, *108*, 2646. (b) Jacobs, C. B.; Peairs, M. J.; Venton, B. J. *Anal. Chim. Acta* **2010**, *662*, 105. (c) Yang, X.; Haubold, L.; DeVivo, G.; Swain, G. M. *Anal. Chem.* **2012**, *84*, 6240. (d) Hawley, M. D.; Tatawawadi, S. V.; Piekarski, S.; Adams, R. N. *J. Am. Chem. Soc.* **1967**, *89*, 447.

(2) (a) Yu, X.; Wang, Q.; Lin, Y.; Zhao, J.; Zhao, C.; Zheng, J. *Langmuir* **2012**, *28*, 6595. (b) Güell, A. G.; Meadows, K. E.; Unwin, P. R.; Macpherson, J. V. *Phys. Chem. Chem. Phys.* **2010**, *12*, 10108. (c) Singh, Y. S.; Sawarynski, L. E.; Michael, H. M.; Ferrell, R. E.; Murphey-Corb, M. A.; Swain, G. M.; Patel, B. A.; Andrews, A. M. *ACS Chem. Neurosci.* **2010**, *1*, 49.

(3) (a) Zhou, M.; Zhai, Y.; Dong, S. *Anal. Chem.* **2009**, *81*, 5603. (b) Wightman, R. M. *Science* **2006**, *311*, 1570. (c) Day, J. J.; Roitman, M. F.; Wightman, R. M.; Carelli, R. M. *Nat. Neurosci.* **2007**, *10*, 1020. (d) Alwarappan, S.; Erdem, A.; Liu, C.; Li, C.-Z. *J. Phys. Chem. C* **2009**, *113*, 8853.

(4) Kneten, K. R.; McCreery, R. L. *Anal. Chem.* **1992**, *64*, 2518.

(5) (a) Bowling, R. J.; Packard, R. T.; McCreery, R. L. *J. Am. Chem. Soc.* **1989**, *111*, 1217. (b) Kachoosangi, R. T.; Compton, R. G. *Anal. Bioanal. Chem.* **2007**, *387*, 2793.

(6) (a) Sudhakara Prasad, K.; Muthuraman, G.; Zen, J.-M. *Electrochem. Commun.* **2008**, *10*, 559. (b) Lim, C. X.; Hoh, H. Y.; Ang, P. K.; Loh, K. P. *Anal. Chem.* **2010**, *82*, 7387. (c) Strand, A. M.; Venton, B. J. *Anal. Chem.* **2008**, *80*, 3708.

(7) (a) Lai, S. C. S.; Dudin, P. V.; Macpherson, J. V.; Unwin, P. R. *J. Am. Chem. Soc.* **2011**, *133*, 10744. (b) Snowden, M. E.; Güell, A. G.; Lai, S. C. S.; McKelvey, K.; Ebejer, N.; O'Connell, M. A.; Colburn, A. W.; Unwin, P. R. *Anal. Chem.* **2012**, *84*, 2483. (c) Ebejer, N.; Schnippering, M.; Colburn, A. W.; Edwards, M. A.; Unwin, P. R. *Anal. Chem.* **2010**, *82*, 9141.

(8) Patten, H. V.; Lai, S. C.; Macpherson, J. V.; Unwin, P. R. *Anal. Chem.* **2012**, *84*, 5427.

(9) Chang, H.; Bard, A. J. *Langmuir* **1991**, *7*, 1143.

(10) Lai, S. C. S.; Patel, A. N.; McKelvey, K.; Unwin, P. R. *Angew. Chem., Int. Ed.* **2012**, *51*, 5405.

(11) (a) Güell, A. G.; Ebejer, N.; Snowden, M. E.; Macpherson, J. V.; Unwin, P. R. *J. Am. Chem. Soc.* **2012**, *134*, 7258. (b) Güell, A. G.; Ebejer, N.; Snowden, M. E.; McKelvey, K.; Macpherson, J. V.; Unwin, P. R. *Proc. Natl. Acad. Sci. U.S.A.* **2012**, *109*, 11487.

(12) (a) DuVall, S. H.; McCreery, R. L. *J. Am. Chem. Soc.* **2000**, *122*, 6759. (b) Bath, B. D.; Michael, D. J.; Trafton, B. J.; Joseph, J. D.; Runnels, P. L.; Wightman, R. M. *Anal. Chem.* **2000**, *72*, 5994.

(13) (a) Anne, A.; Cambril, E.; Chovin, A.; Demaille, C.; Goyer, C. *ACS Nano* **2009**, *3*, 2927. (b) Edwards, M. A.; Bertoncello, P.; Unwin, P. R. *J. Phys. Chem. C* **2009**, *113*, 9218. (c) Williams, C. G.; Edwards, M. A.; Colley, A. L.; Macpherson, J. V.; Unwin, P. R. *Anal. Chem.* **2009**, *81*, 2486. (d) Frederix, P. L.; Bosshart, P. D.; Akiyama, T.; Chami, M.; Gullo, M. R.; Blackstock, J. J.; Dooleweerdt, K.; de Rooij, N. F.; Staufer, U.; Engel, A. *Nanotechnology* **2008**, *19*, No. 384004.

(14) Patel, A. N.; Collignon, M. G.; O'Connell, M. A.; Hung, W. O. Y.; McKelvey, K.; Macpherson, J. V.; Unwin, P. R. *J. Am. Chem. Soc.* **2012**, DOI: 10.1021/ja308615h.

(15) (a) Hazimeh, H.; Nunige, S.; Cornut, R.; Lefrou, C.; Combellas, C.; Kanoufi, F. *Anal. Chem.* **2011**, *83*, 6106. (b) Nunige, S.; Cornut, R.; Hazimeh, H.; Hauquier, F.; Lefrou, C.; Combellas, C.; Kanoufi, F. *Angew. Chem., Int. Ed.* **2012**, *51*, 5208. (c) Shan, X.; Patel, U.; Wang, S.; Iglesias, R.; Tao, N. *Science* **2010**, *327*, 1363.